43rd AIAA Aerospace Sciences Meeting and Exhibit
10 - 13 January 2005, Reno, Nevada

AIAA 2005-604

Installation Effects on the Flow and Noise of an Under-the-Wing Mounted Dual Stream Jet

Nikolai N. Pastouchenko* and Christopher K.W. Tam†
Florida State Univeristy, Tallahassee, FL 32306-4510

It is known experimentally that a jet mounted under a wing generates more noise than the same jet in isolation. The excess noise is referred to as installation noise. Installation noise is largely of aerodynamic origin. The principal mechanism is believed to be the impact of the downwash of the wing-flap on the jet flow. The downwash causes the jet to deflect downward and to distort laterally. This brings about an increase in turbulence in the jet. The increase in the level of turbulence, in turn, leads to the emission of additional noise. The modeling and computation of the downwash, the distorted jet flow and the excess noise radiation are the objectives of this investigation. It will be shown that calculated results at high frequencies compare well with experimental measurements.

I. Introduction

IT is known experimentally, since the late seventies, that a jet installed under a wing of an aircraft radiates more noise than the same jet in a stand-alone condition. The excess noise is the propulsion-airframe integration noise or commonly referred to as installation noise. When a jet is placed near a wing, there is an increase in noise in the fly-over directions because of the reflection of sound by the wing. Here, installation noise includes not merely the noise increase due to the reflection of sound by the wing. The major part of this noise is generated aerodynamically by the nonlinear interaction between the flow around the wing-flap and the jet. In this work, our primary interest is to model and to predict installation noise of aerodynamic origin. Installation noise increases not only the total aircraft noise in the fly-over plane but also in the sideline directions. It is especially important during landings and take-offs when the flaps are down.

During the eighties, a number of experiments were carried out trying to quantify the characteristics and intensity of installation noise[1-4]. Most of these experiments involved the measurements of the jet alone noise and the noise when the jet was placed near a model of an aircraft wing inside an anechoic chamber. The experimental measurements by Wang[2] were the most systematic. In his experiment, a scaled model of the wing of a DC-10 aircraft was used. Large noise increase was observed in the fly-over plane in the low frequency part of the spectrum. The increase in high frequency noise was less. In directions at small exhaust angles, the installation noise intensity was quite low. In the sideline, the radiated noise characteristics, on the other hand, were quite different. Overall, the measured data indicated that installation noise had a unique spectral shape and a directional pattern of its own.

Recently, there is a renewed interest in propulsion-airframe integration noise. Mead & Strange[5] investigated the under-the-wing installation effects on jet noise with special emphasis on the sideline directions. Their interest in the sideline was motivated by the experience that it was generally more difficult to meet legislative limit on sideline noise level requirements. They reported the measurement of high installation noise level in the low frequency range.

One drawback of the Mead & Strange experiment as well as most of the previous works is that the experiments were carried out in static conditions. Upon realizing that the effect of forward flight is extremely important in the interaction between the flow around the wing-flap and the jet, a series of new experiments on installation noise was conducted by engineers of the Boeing Company; Shivashankara & Blackner[6], Blackner & Bhat[7] and Bhat & Blackner[8]. They employed an open wind tunnel at M=0.28 to simulate the forward motion of the aircraft. By using elliptic mirror microphones and the newly developed phase array microphones, they were able to obtain noise source location maps as well as far field noise data.

In the Boeing study, summarized by Bhat[9], the variation and sensitivity of installation noise to a range of flow parameters, wing-flap settings, jet engine location and pitching angle were investigated. Installation noise up to 6 dB

* Postdoctoral Research Associate, Department of Mathematics.
† Robert O. Lawton Distinguished Professor, Department of Mathematics, Fellow AIAA.

across a wide band of frequency was measured. This is a very large increase in noise. It can easily negate the gains of recent successes in suppressing other components of airframe noise.

Below is a summary of the important findings of the Boeing investigation.

1. The presence of the airframe increases jet noise significantly.
2. The noise increase follows monotonically with increasing flap deflection. Flap deflection has the largest effect on installation noise.
3. Noise levels are insensitive to engine installation location within Boeing's current envelope of possibilities at takeoff flap setting.
4. A wide bifurcation can contribute to a slight increase in noise level.
5. Pitching the nozzle up toward the wing can increase the noise levels, while pitching the nozzle away from the wing has little benefit.

In conjunction with their experimental study, an empirical installation noise prediction method was developed by Bhat & Blackner[8]. The approach of Bhat & Blackner followed an earlier work at Boeing by Lu[10] for the prediction of noise from isolated coaxial jets in ambient flow. The methodology is entirely empirical. Only a limited amount of flow physics was incorporated into the formulation of the prediction code. The predicted noise spectra were in fair agreements with measurements at low to moderate frequencies. However, there were significant discrepancies in the higher frequency range of all the measured spectra.

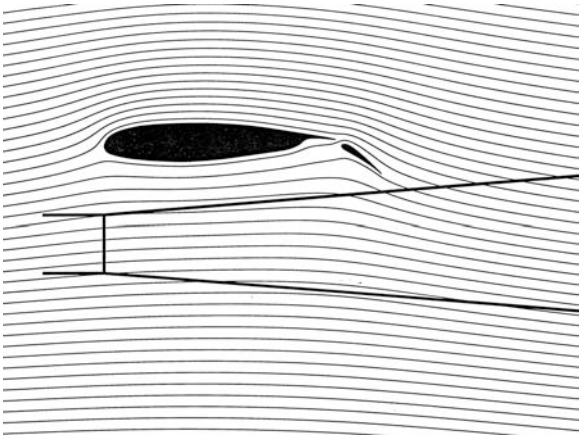

Figure 1. Streamlines showing the impact of downwash on an under-the-wing mounted jet

The primary objective of this investigation is to develop a computational model to calculate installation effects on the flow and noise of an under-the-wing mounted dual stream jet. Installation of a jet engine under a wing in forward flight leads to very complex fluid dynamical interaction between the flow around the wing-flap and the jet. To compute the entire interaction is beyond the scope of this work. Based on the Boeing results, we focus our attention mainly on the impact of the downwash of the wing-flap on the jet plume. Figure 1 shows the streamlines around an airfoil at zero angle of attack and a flap at a deflection angle of 35 degrees. The forward flight Mach number is 0.2. Superimposed on this figure are the outlines of a nozzle and that of a Mach 0.8 jet at a temperature ratio of 1.54. This figure indicates that the downwash, which is especially strong when the flap is fully deployed, could cause the jet to deflect downward and distorted laterally. In the present investigation, a simple mathematical model is adopted in the computation. Only the effect of downwash on the jet is considered. The effect of the presence of the jet on the wing-flap flow will be neglected. The large deflection and distortion of the jet caused by the strong downwash lead to an increase in the level of turbulence in the jet. This, in turn, leads to an increase in jet noise radiation. It is known that there are two principal components of jet mixing noise. One component is generated by the large turbulence structures of the jet flow and the other component is generated by the fine scale turbulence. In this work, only the installation noise from the enhanced fine scale turbulence is calculated. Comparisons with experimental measurements will be reported.

The rest of the paper is as follows. First, the downwash from the wing-flap is calculated by solving the Euler equations. The distorted jet mean flow is then calculated by a parabolized RANS *k–e* turbulence model taking into consideration the downwash as a side boundary condition. The computed mean flow and the turbulence information from the *k–e* model are subsequently used to calculate the radiated noise through the extended Tam & Auriault fine scale turbulence noise theory[11,12]. Finally, the installation noise is determined by subtracting from the calculated noise the noise of the same jet in isolation.

II. Downwash from a Wing-Flap in High-Lift Configuration

For the purpose of calculating the downwash of a wing-flap combination in an approach configuration, an inviscid flow model is used. The wing will be taken as two-dimensional. The governing equations are the Euler and energy equations,

$$\frac{\partial \rho}{\partial t} + \rho\left(\frac{\partial u}{\partial x} + \frac{\partial v}{\partial y}\right) + u\frac{\partial \rho}{\partial x} + v\frac{\partial \rho}{\partial y} = 0 \tag{1}$$

$$\frac{\partial u}{\partial t} + u\frac{\partial u}{\partial x} + v\frac{\partial u}{\partial y} + \frac{1}{\rho}\frac{\partial p}{\partial x} = 0 \tag{2}$$

$$\frac{\partial v}{\partial t} + u\frac{\partial u}{\partial x} + v\frac{\partial u}{\partial y} + \frac{1}{\rho}\frac{\partial p}{\partial y} = 0 \tag{3}$$

$$\frac{\partial p}{\partial t} + u\frac{\partial p}{\partial x} + v\frac{\partial p}{\partial y} + \rho\left(\frac{\partial u}{\partial x} + \frac{\partial v}{\partial y}\right) = 0\,. \tag{4}$$

The boundary condition on the surface of the wing-flap is,

$$un_x + vn_y = 0 \tag{5}$$

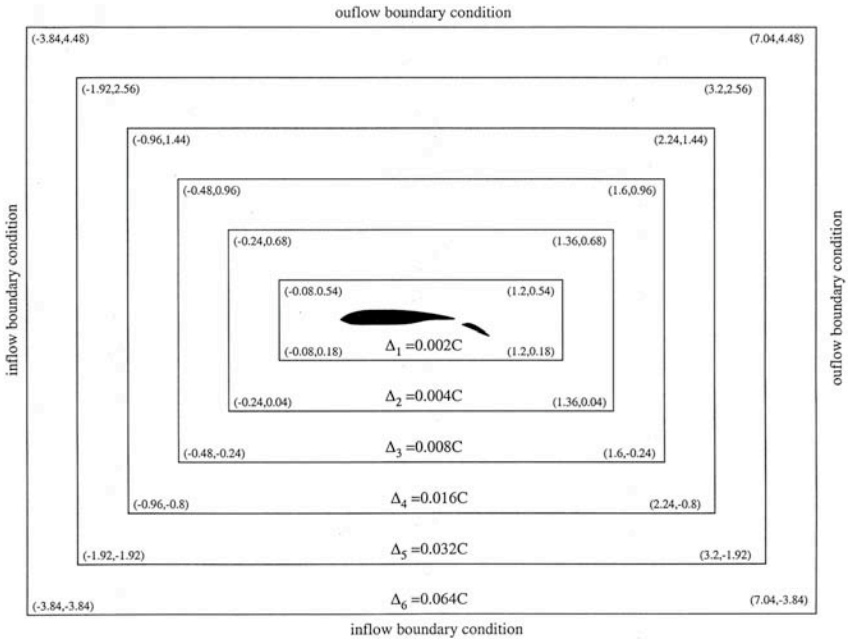

Figure 2. Computation domain for calculating the downwash of an airfoil and flap

where $n=(n_x,n_y)$ is the unit normal of the wing-flap surface.

In the present study, equations (1) to (4) are solved by the Multi-size-mesh Multi-time-step Dispersion-Relation-Preserving scheme[13] on a Cartesian grid as shown in figure 2. The finest mesh is employed in the block containing the airfoil and the flap. This very fine mesh is used to resolve the geometrical details of the two solid bodies. Away from the airfoil, the flow becomes more and more smooth. Thus, there is a gradual relaxation of the resolution requirement. Accordingly, the mesh size and the corresponding time step used in the computation increase by a factor of two each time one moves to the next outer block. In this way, the flow over a fairly large domain can be computed with a reasonable amount of computing time.

To enforce boundary condition (5), the Cartesian boundary treatment method proposed by Kurbatskii & Tam[14] is used. At the inflow and lower boundaries of the computation domain, the radiation boundary condition of Tam & Webb[15] is enforced. At the right and top boundaries, the Tam & Webb[15] outflow boundary conditions are implemented. The computation starts with a uniform flow and time marched to steady state. To promote fast convergence, the method of accelerated convergence to steady state proposed by Tam & Dong[16] is applied. The idea of the method is to perform a "canceling-the-residue" operation. In a numerical computation, the best one can do is to make the difference between the numerical and the exact solution to be of the order of a tenth of a percent. In other words, further time marching computation could be a waste of effort in terms of improving the accuracy of the solution, once the residual reaches a level of the order of 10^{-5}. With this in mind, it is possible to add a term that is exactly equal in magnitude but opposite in sign to the residual, at this stage, to the right side of each of the governing equations. These are terms of order 10^{-5} or less and would, therefore, not materially affecting the accuracy of the steady state numerical solution. The added terms may be regarded as minute artificial distributed sources of fluid, momentum or heat. The consequence of adding these source terms is to cancel the residuals instantly to zero. Of course, for the multi-level matching scheme, the residuals of the scheme are greatly reduced in this way but they would not exactly equal to zero at the next time level. Numerical experiments indicate that when the above canceling-the-residual procedure is performed, the overall residuals of the computation drop almost

instantaneously by several orders of magnitude. This operation may be applied repeatedly until the residuals are driven to machine round-off error.

III. Computation of the Mean Flow of an Under-the-Wing Mounted Jet

We will use the Reynolds Averaged Navier-Stokes Equations (RANS) together with the k–ε turbulence model to calculate the mean flow of an under-the-wing mounted dual stream jet. It has been pointed out that the standard k–ε model has a number of deficiencies. To remedy the shortcomings of the model, we will include the Pope correction[17] for three-dimensional flows, the Sarkar correction[18] for convective Mach number effects and the Tam & Ganesan[19] correction for density gradients existing in hot jets.

A. Parabolized RANS Equations

For convenience, nondimensional variables with respect to the following scales are used.

length scale = D_p (diameter of primary nozzle)
velocity scale = u_p (fully expanded velocity of primary jet)
time scale = D_p / u_p
density scale = ρ_p (density of primary nozzle)
pressure scale = $\rho_p u_p^2$
temperature scale = T_p (fully expanded temperature of primary jet)
scale for k and τ_{ij} = u_p^2
scale for ε = u_p^3 / D_p
scale for μ_t = $D_p u_p$

The steady state RANS equations including the modified k–ε turbulence model in Cartesian tensor notation are,

$$\frac{\partial u_j}{\partial x_j} - \frac{u_j}{T}\frac{\partial T}{\partial x_j} + \frac{u_j}{p}\frac{\partial p}{\partial x_j} = 0 \tag{6}$$

$$\rho u_j \frac{\partial u_i}{\partial x_j} = -\frac{\partial p}{\partial x_i} - \frac{\partial}{\partial x_j}\left(\rho \tau_{ij}\right) \tag{7}$$

$$\rho u_j \frac{\partial T}{\partial x_j} = -\rho(\gamma - 1) M_p^2 p \frac{\partial u_j}{\partial x_j} + \rho(\gamma - 1) M_p^2 \Phi + \frac{1}{\sigma_T}\frac{\partial}{\partial x_j}\left(\left(\mu + \mu_t\right)\frac{\partial T}{\partial x_j}\right) \tag{8}$$

$$\rho u_j \frac{\partial k}{\partial x_j} = \rho \tau_{ij} \frac{\partial u_i}{\partial x_j} - \rho\varepsilon + \frac{1}{\sigma_k}\frac{\partial}{\partial x_j}\left(\left(\mu + \mu_t\right)\frac{\partial k}{\partial x_j}\right) \tag{9}$$

$$\rho u_j \frac{\partial \varepsilon_s}{\partial x_j} = -c_{\varepsilon 1}\frac{\varepsilon_s}{k}\rho \tau_{ij}^{(s)} \frac{\partial u_i}{\partial x_j} - \left(c_{\varepsilon 2} - c_{\varepsilon 3}\right)\rho\frac{\varepsilon_s^2}{k} + \frac{1}{\sigma_\varepsilon}\frac{\partial}{\partial x_j}\left(\left(\mu + \mu_t^{(s)}\right)\frac{\partial \varepsilon_s}{\partial x_j}\right) \tag{10}$$

$$p = \frac{\rho T}{\gamma M_p^2} \tag{11}$$

$$\mu = \mu_s\left(1 + \alpha_1 M_t^2\right), \qquad M_t^2 = \frac{2kM_p^2}{T} \tag{12}$$

$$\tau_{ij} = \frac{2}{3}k\delta_{ij} - \nu_t\left(\frac{\partial u_i}{\partial x_j} + \frac{\partial u_j}{\partial x_i} - \frac{2}{3}\frac{\partial u_k}{\partial x_k}\delta_{ij}\right) \tag{13a}$$

$$\tau_{ij}^{(s)} = \frac{2}{3}k\delta_{ij} - \nu_t^{(s)}\left(\frac{\partial u_i}{\partial x_j} + \frac{\partial u_j}{\partial x_i} - \frac{2}{3}\frac{\partial u_k}{\partial x_k}\delta_{ij}\right) \tag{13b}$$

$$\nu_t = c_\mu \frac{k^2}{\varepsilon} + \nu_\varepsilon, \qquad \nu_t^{(s)} = c_\mu \frac{k^2}{\varepsilon_s} + \nu_\varepsilon^{(s)} \tag{14a}$$

$$\nu_\varepsilon = \begin{cases} c_\varepsilon \dfrac{k^{7/2}}{\varepsilon^2}\dfrac{|\nabla\varepsilon\cdot\nabla u|}{\varepsilon|\nabla u|}, & \text{if } (\nabla\varepsilon)\cdot(\nabla u) \text{ is negative} \\ 0, & \text{otherwise} \end{cases} \tag{14b}$$

$$\nu_\varepsilon^{(s)} = \begin{cases} c_\varepsilon \dfrac{k^{7/2}}{\varepsilon_s^2}\dfrac{|\nabla\varepsilon\cdot\nabla u|}{\varepsilon|\nabla u|}, & \text{if } (\nabla\varepsilon)\cdot(\nabla u) \text{ is negative} \\ 0, & \text{otherwise} \end{cases} \tag{14c}$$

$$\varepsilon = \tau_{ij}\tau_{jk}s_{ki} \tag{15a}$$

$$\tau_{ij} = \frac{1}{2}\frac{k}{\varepsilon_s}\left(\frac{\partial u_i}{\partial x_j} - \frac{\partial u_j}{\partial x_i}\right) \tag{15b}$$

$$s_{ij} = \frac{1}{2}\frac{k}{\varepsilon_s}\left(\frac{\partial u_i}{\partial x_j} + \frac{\partial u_j}{\partial x_i}\right). \tag{15c}$$

The empirical constants of the above equations are assigned the values below.

$$c_\mu = 0.0874, \qquad c_{\varepsilon 1} = 1.40, \qquad c_{\varepsilon 2} = 2.02, \qquad c_{\varepsilon 3} = 0.822$$

$$\sigma_T = \Pr \text{ (turbulent Prandtl number)} = 0.422$$

$$\sigma_k = 0.324, \qquad \sigma_\varepsilon = 0.377, \qquad \sigma_1 = 0.518, \qquad c_\varepsilon = 0.035.$$

It is advantageous to separate the solution into two parts as,

$$\begin{pmatrix} p \\ T \\ u_i \end{pmatrix} = \begin{pmatrix} p^{(a)} \\ T^{(a)} \\ u_i^{(a)} \end{pmatrix} + \begin{pmatrix} \hat{p} \\ \hat{T} \\ \hat{u}_i \end{pmatrix} \tag{16}$$

where the quantities with superscript (*a*) are the downwash flow solution found in the previous section. Here it will be assumed that this solution has been completed at this stage and that the main effort now is to calculate $(\hat{p},\hat{T},\hat{u}_i)$. The principal reason for separating the solution in the form of (16) is to allow a clear and simple prescription of boundary conditions. Here the natural boundary conditions are,

$$\left(\hat{p},\hat{T},\hat{u}_i,k,\varepsilon\right) \to 0, \quad \text{away from the jet}. \tag{17}$$

In this investigation, the aim is to develop a set of parabolized equations for the determination of unknown variables $(\hat{p},\hat{T},\hat{u}_i,k,\varepsilon)$. The approach is similar to previous works[12,20,21]. But because of the downwash flow, the resulting equations are different. To simplify the derivation of the parabolized equations, it will be assumed that the downwash flow is practically incompressible; i.e.,

$$\frac{\partial u_j^{(a)}}{\partial x_j} = 0 \tag{18}$$

and that ρ in equations (2) and (3) may be substituted by ρ_∞. This approximation is justified since the forward flight Mach number is low subsonic.

In Ref. [12,20,21], the fluid density is eliminated by using the equation of state in favor of pressure p and temperature T. Here the same strategy is followed. Thus, (16), which is the continuity equation, is used to compute $\hat{p}$. Substitution of (16) into (6) and after some algebraic manipulation, it is straightforward to derive a parabolized equation for $\hat{p}$ in Cartesian coordinates. The x-axis is in the flow direction

$$\begin{aligned}\frac{\partial \hat{p}}{\partial x} = &-\frac{\partial p^{(a)}}{\partial x} + \frac{1}{\left(\hat{u}+u^{(a)}\right)}\left[-\left(\hat{v}+v^{(a)}\right)\left(\frac{\partial \hat{p}}{\partial y}+\frac{\partial p^{(a)}}{\partial y}\right) - \hat{w}\frac{\partial \hat{p}}{\partial z} - \left(\hat{p}+p^{(a)}\right)\left(\frac{\partial \hat{u}}{\partial x}+\frac{\partial \hat{v}}{\partial y}+\frac{\partial \hat{w}}{\partial z}\right)\right.\\ &\left.+\frac{\gamma}{\gamma M_p^2}\left(\left(\hat{u}+u^{(a)}\right)\frac{\partial \hat{T}}{\partial x}+\left(\hat{v}+v^{(a)}\right)\frac{\partial \hat{T}}{\partial y}+\hat{w}\frac{\partial \hat{T}}{\partial z}\right)\right]\end{aligned} \tag{19}$$

where $(\hat{u},\hat{v},\hat{w})$ are the Cartesian velocity components. It is to be noted that the terms $\partial\hat{u}/\partial x$ and $\partial\hat{T}/\partial x$ on the right side of (19) are given by the x-momentum and the energy equation (see equations (20) and (23) below), so that the right side does not have any unknown x-derivative.

On following the steps in the derivation of (19) and by making use of approximation (18) and boundary layer argument; i.e., $\partial/\partial y$, $\partial/\partial z >> \partial/\partial x$, a full set of parabolized equations for variables $(\hat{u},\hat{v},\hat{w},\hat{T},k,\varepsilon)$ can be derived readily. These equations when written out are as follows

$$\frac{\partial \hat{u}}{\partial x} = \frac{1}{\left(\hat{u}+u^{(a)}\right)}\left[-\left(\hat{v}+v^{(a)}\right)\frac{\partial \hat{u}}{\partial y} - \hat{w}\frac{\partial \hat{u}}{\partial z} - \hat{u}\frac{\partial u^{(a)}}{\partial x} - \hat{v}\frac{\partial u^{(a)}}{\partial y} + \frac{\rho_\infty}{\rho}\frac{\partial p^{(a)}}{\partial x} - \frac{1}{\rho}\left(\frac{\partial\left(\rho\hat{\tau}_{xy}\right)}{\partial y}+\frac{\partial\left(\rho\hat{\tau}_{xz}\right)}{\partial z}\right)\right] \tag{20}$$

$$\frac{\partial \hat{v}}{\partial x} = \frac{1}{\left(\hat{u}+u^{(a)}\right)}\left[-\left(\hat{v}+v^{(a)}\right)\frac{\partial \hat{v}}{\partial y} - \hat{w}\frac{\partial \hat{v}}{\partial z} - \hat{u}\frac{\partial v^{(a)}}{\partial x} - \hat{v}\frac{\partial v^{(a)}}{\partial y} - \frac{1}{\rho}\frac{\partial \hat{p}}{\partial y} + \frac{\rho_\infty}{\rho}\frac{\partial p^{(a)}}{\partial y} - \frac{1}{\rho}\left(\frac{\partial\left(\rho\hat{\tau}_{yy}\right)}{\partial y}+\frac{\partial\left(\rho\hat{\tau}_{yz}\right)}{\partial z}\right)\right] \tag{21}$$

$$\frac{\partial \hat{w}}{\partial x} = \frac{1}{\left(\hat{u}+u^{(a)}\right)}\left[-\left(\hat{v}+v^{(a)}\right)\frac{\partial \hat{w}}{\partial y} - \hat{w}\frac{\partial \hat{w}}{\partial z} - \frac{1}{\rho}\frac{\partial \hat{p}}{\partial z} - \frac{1}{\rho}\left(\frac{\partial\left(\rho\hat{\tau}_{xy}\right)}{\partial y}+\frac{\partial\left(\rho\hat{\tau}_{zz}\right)}{\partial z}\right)\right] \tag{22}$$

$$\begin{aligned}\frac{\partial \hat{T}}{\partial x} = &\frac{1}{\left(\hat{u}+u^{(a)}\right)}\left[-\left(\hat{v}+v^{(a)}\right)\frac{\partial \hat{T}}{\partial y} - \hat{w}\frac{\partial \hat{T}}{\partial z} - (\gamma-1)\left(\hat{T}+T\right)\left(\frac{\partial \hat{u}}{\partial x}+\frac{\partial \hat{v}}{\partial y}+\frac{\partial \hat{w}}{\partial z}\right) + \gamma(\gamma-1)M_p^2\varepsilon\right.\\ &\left.+\frac{\gamma}{P_r}\left(\frac{\partial}{\partial y}\left(\nu_t\frac{\partial \hat{T}}{\partial y}\right)+\frac{\partial}{\partial z}\left(\nu_t\frac{\partial \hat{T}}{\partial z}\right)\right)\right]\end{aligned} \tag{23}$$

$$\frac{\partial k}{\partial x} = \frac{1}{\left(\hat{u}+u^{(a)}\right)}\Big[\left(\hat{v}+v^{(a)}\right)\frac{\partial k}{\partial y} + \hat{w}\frac{\partial k}{\partial z} - \tau_{xy}\left(\frac{\partial \hat{u}}{\partial y}+\frac{\partial u^{(a)}}{\partial y}\right) - \tau_{xz}\frac{\partial \hat{u}}{\partial z} - \tau_{yy}\left(\frac{\partial \hat{v}}{\partial y}+\frac{\partial v^{(a)}}{\partial y}\right) - \tau_{yz}\frac{\partial \hat{v}}{\partial z} - \tau_{zy}\frac{\partial \hat{w}}{\partial y} - \tau_{zz}\frac{\partial \hat{w}}{\partial z} - \varepsilon + \frac{1}{\sigma_k}\left(\frac{\partial}{\partial y}\left(\mu+\mu_t\frac{\partial k}{\partial y}\right) + \frac{\partial}{\partial z}\left(\mu+\mu_t\frac{\partial k}{\partial z}\right)\right)\Big] \tag{24}$$

$$\frac{\partial \varepsilon}{\partial x} = \frac{1}{\left(\hat{u}+u^{(a)}\right)}\Big[\left(\hat{v}+v^{(a)}\right)\frac{\partial \varepsilon}{\partial y} + \hat{w}\frac{\partial \varepsilon}{\partial z} - c_{\varepsilon 1}\frac{\varepsilon}{k}\left(\tau_{xy}^{(s)}\left(\frac{\partial \hat{u}}{\partial y}+\frac{\partial u^{(a)}}{\partial y}\right) + \tau_{xz}^{(s)}\frac{\partial \hat{u}}{\partial z} + \tau_{yy}^{(s)}\left(\frac{\partial \hat{v}}{\partial y}+\frac{\partial v^{(a)}}{\partial y}\right) + \tau_{yz}^{(s)}\frac{\partial \hat{v}}{\partial z} + \tau_{zy}^{(s)}\frac{\partial \hat{w}}{\partial y} + \tau_{zz}^{(s)}\frac{\partial \hat{w}}{\partial z}\right) - \left(c_{\varepsilon 2} - c_{\varepsilon 3}\right)\frac{\varepsilon^2}{k} + \frac{1}{\sigma_\varepsilon}\left(\frac{\partial}{\partial y}\left(\mu+\mu_t^{(s)}\frac{\partial \varepsilon}{\partial y}\right) + \frac{\partial}{\partial z}\left(\mu+\mu_t^{(s)}\frac{\partial \varepsilon}{\partial z}\right)\right)\Big] \tag{25}$$

where ρ_∞ and T_∞ are the density and temperature of the free stream. To complete the parabolized system, all the x-derivatives in the stress terms and c of (13) and (15) are dropped. They are small compared to the y and z derivative terms.

B. Radiation or Outgoing Wave Boundary Conditions

To compute the solution of the parabolized system of equations (19) to (25), the 4-level Dispersion-Relation-Preserving (DRP) scheme[15] is used to march the solution downstream in the x-direction. Here, the x-axis is treated as the time axis in the DRP methodology. The solution is contained in planes parallel to the x–z plane. The computation domain in these parallel planes is finite and does not extend too far from the jet flow. For this reason, boundary condition (17) for the variables $(\hat{p},\hat{T},\hat{u}_i)$ cannot be implemented. As in previous work involving the computation of jet mean flow through parabolized equations[22], a set of radiation/outgoing wave boundary conditions is used at the edge of the computation domain. This set of boundary conditions is derived by first finding an asymptotic solution (an approximate one if necessary) of the parabolized equations in the limit $(y^2+z^2)^{1/2}$ is large. The radiation boundary conditions are then found by eliminating the unknown function of the asymptotic solution through cross differentiation. In this work, this procedure has been carried out with the aid of a frozen coefficient approximation. The boundary conditions for large $(y^2+z^2)^{1/2}$ actually implemented in this work are,

$$u^{(a)}\frac{\partial \hat{u}}{\partial x} + v^{(a)}\frac{\partial \hat{u}}{\partial y} = 0 \tag{26}$$

$$u^{(a)}\frac{\partial \hat{v}}{\partial x} + v^{(a)}\frac{\partial \hat{v}}{\partial y} + a\left[\frac{z}{\left(z^2+y^2\right)^{\frac{1}{2}}}\frac{\partial \hat{v}}{\partial z} + \frac{y}{\left(z^2+y^2\right)^{\frac{1}{2}}}\frac{\partial \hat{v}}{\partial y} + \frac{z^2}{\left(y^2+z^2\right)^{\frac{3}{2}}}\left(\hat{v} - \frac{v^{(a)}}{u^{(a)}}\hat{u}\right)\right] - \frac{yz}{\left(y^2+z^2\right)^{\frac{3}{2}}}\hat{w} + \frac{\hat{v} - v^{(a)}\hat{u}/u^{(a)}}{\left(y^2+z^2\right)^{\frac{1}{2}}} = 0 \tag{27}$$

$$u^{(a)}\frac{\partial \hat{w}}{\partial x} + v^{(a)}\frac{\partial \hat{w}}{\partial y} + a\left[\frac{z}{\left(y^2+z^2\right)^{\frac{1}{2}}}\frac{\partial \hat{w}}{\partial z} + \frac{y}{\left(y^2+z^2\right)^{\frac{1}{2}}}\frac{\partial \hat{w}}{\partial y} + \frac{y^2}{\left(y^2+z^2\right)^{\frac{3}{2}}}\hat{w} - \frac{yz}{\left(y^2+z^2\right)^{\frac{3}{2}}}\left(\hat{v} - \frac{v^{(a)}}{u^{(a)}}\hat{u}\right) + \frac{\hat{w}}{\left(y^2+z^2\right)^{\frac{1}{2}}}\right] = 0 \tag{28}$$

$$\left[u^{(a)}\frac{\partial}{\partial x} + v^{(a)}\frac{\partial}{\partial y} + a\left[\frac{z}{\left(y^2+z^2\right)^{\frac{1}{2}}}\frac{\partial}{\partial x} + \frac{y}{\left(y^2+z^2\right)^{\frac{1}{2}}}\frac{\partial}{\partial y}\right] + \frac{1}{\left(y^2+z^2\right)^{\frac{1}{2}}}\right]\begin{bmatrix}\hat{p}\\ \hat{T}\end{bmatrix} = 0 \tag{29}$$

$$k = \square_k = 0. \tag{30}$$

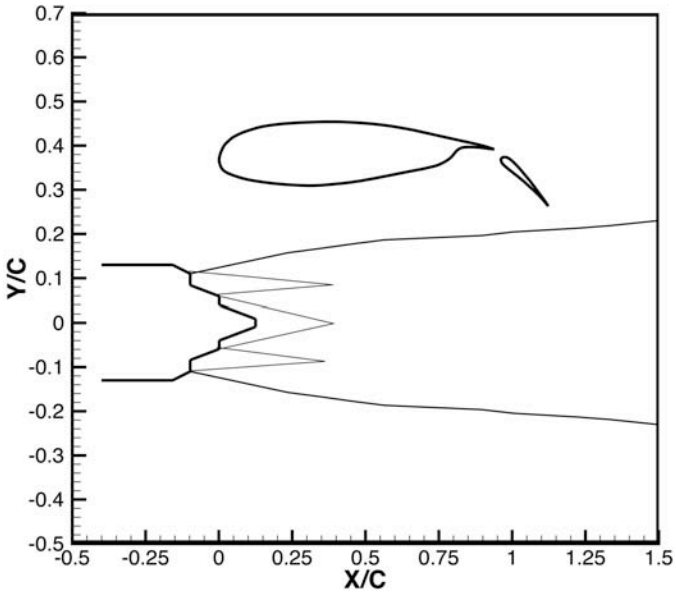

Figure 3. Installed jet model. C = length of wing chord.

C. Numerical Results

Consider an under-the-wing mounted dual stream jet in a configuration as shown in figure 3. The nozzle has an area ratio of 3 and is designed to operate at a bypass ratio of 6 with primary jet Mach number, M_p=0.762, temperature ratio T_p/T_a=2.9 (T_p is the reservoir temperature of the primary jet, T_a is the ambient temperature) and secondary jet Mach number, M_s=0.9, and temperature ratio T_p/T_a=1.2. The geometry of the nozzle that is used in the Boeing experiments[8], is shown in figure 4.. To illustrate the effect of wing-flap downwash on the jet flow, we consider the case of forward flight Mach number 0.28. As shown in figure 3, the nozzle exit is located directly under the leading edge of the wing, so that there is little downwash flow. The trailing edge of the deflected flap is located at a distance of approximately 3 D_s (D_s = diameter of secondary nozzle) downstream. At this location, the downwash is at the maximum intensity. For the jet mean flow calculation, use is made of the oblique Cartesian coordinates method of Ref. [22]. Computation starts at the exit of the secondary nozzle and marches downstream to the tip of the plug nozzle. This solution provides the starting values for the present computation using parabolized RANS equations (19) to (25) and boundary conditions (26) to (30).

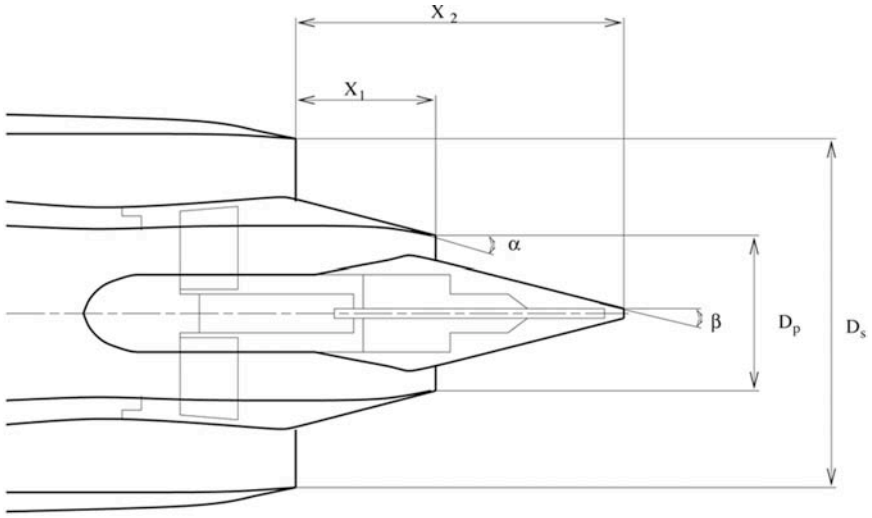

Figure 4. Dual stream nozzle with an external plug of the Boeing experiments. Area ratio = 3, D_s/D_p=1.9, X_1/D_p=0.85, X_2/D_p=1.8, α=14°, β=15°

Figure 5 shows the computer contours of constant axial velocity at different distance downstream on planes parallel to the nozzle exit plane or the *y*–*z*-plane. The two black concentric circles in figures 5a and 5f are the inner and outer boundaries of the primary jet at the nozzle exit. They provide a reference to show the downward displacement of the jet flow. Figures 5a and 5b show the axial velocity contours at x/D_s=1.5 and 3.5. The contours are nearly circular indicating the fact that the impact of wing-flap downwash has not been felt by the jet flow. Figures 5c to 5f show a gradual downward displacement of the jet. At the same time, the jet is distorted laterally. The downward deflection and lateral distortion are responsible for an increase in turbulence level in the jet. Figure 6 show the computed axial velocity profiles of the jet in the vertical symmetry plane through the center of the jet at various distance downstream. These profiles are shown in dotted lines. For comparison purposes, the profiles of the same jet in a stand-alone condition are shown in full lines. It is readily seen that the velocity profiles are displaced gradually downward. In addition, the profiles are no longer symmetric with respect to the maximum velocity point. In a Boeing experiment[7], the downward displacement, as well as the lateral distortion, of the jet were observed. However, not enough quantitative information was provided to allow a direct comparison with computed results.

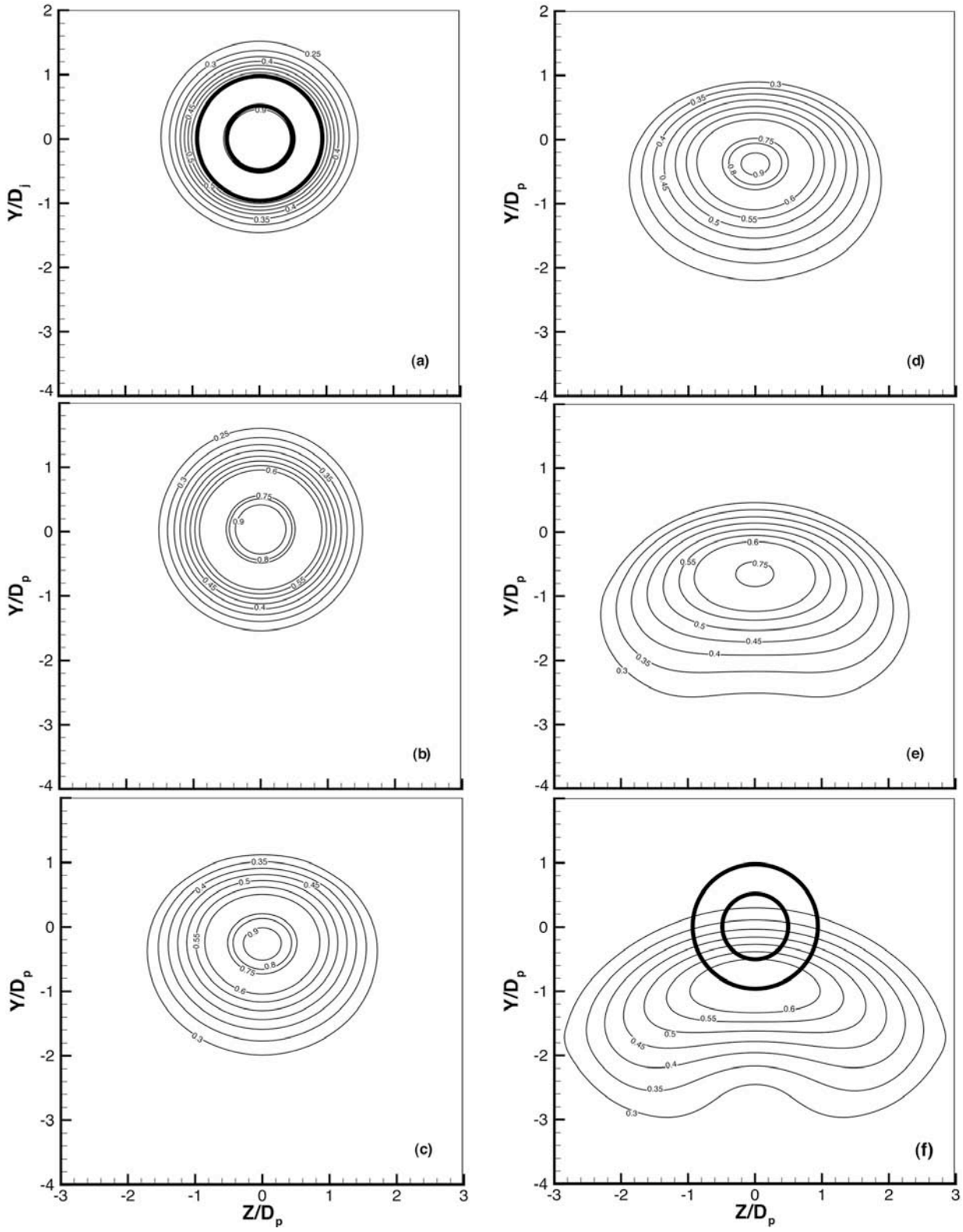

Figure 5. Contours of axial velocity of a dual stream. Flap deflection angle 35°. M_p=0.762, T_p/T_a=2.9; M_s=0.9, T_s/T_a=1.2, M_f=0.28. Area ratio 3, bypass ratio 6 dual stream nozzle. (a) X/D_s=1.5, (b) 3.5, (c) 8.5, (d) 10.5, (e) 15.5, (f) 20.5.

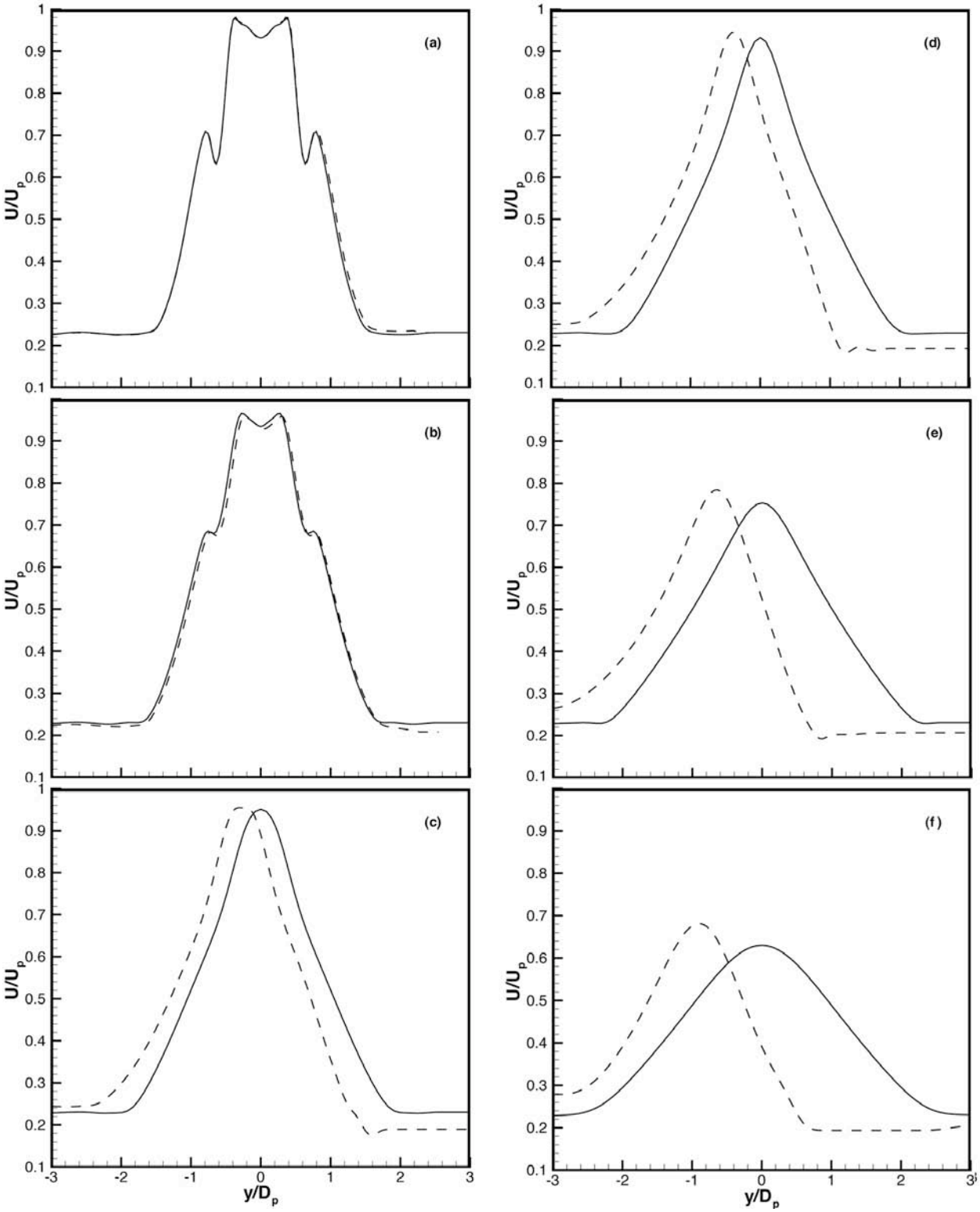

Figure 6. Comparisons between velocity profiles in the vertical plane through the center of the jet. ——— isolated jet, – – – – – under-the-wing mounted dual stream jet with flap at 35° deflection angle. Jet operating conditions and downstream locations are the same as the previous figure.

IV. Computation of Installation Noise and Comparison with Experiment

Once the mean flow of an installed jet and the values of k and ε are computed, the fine scale turbulence noise from the jet may be calculated by the extended Tam & Auriault theory[11,12]. The far field noise spectrum, $S(R,\theta,\phi,fD_p/u_p)$. at a point with spherical polar coordinates (R,θ,ϕ), with respect to a polar coordinate system centered at the nozzle exit with the polar axis coinciding with the x-axis, is given by (in dB),

$$S\left(R,\theta,\phi,\frac{fD_p}{u_p}\right) = 10\log\left(\frac{4\pi S(\mathbf{x},\omega)}{p_{\text{ref}}^2\left(\frac{D_p}{u_p}\right)}\right) \tag{31}$$

where

$$S(\mathbf{x},\omega) = \frac{4\pi^3}{(\ln 2)^{\frac{3}{2}}}\int_{\text{Volume of jet}} \frac{\Gamma\left(\alpha+\frac{1}{2}\right)}{\Gamma(\alpha)}\frac{\hat{q}_s^2}{c^2}\ell_s^3 \frac{\left|p_a(\mathbf{x_2},\mathbf{x},\omega)\right|^2 e^{-\frac{\omega^2\ell_s^2}{\bar{u}^2 4(\ln 2)}}}{\left(1+\omega^2\tau_s^2\left(1-\frac{\bar{u}}{a}\cos\theta\right)^2\right)^{\alpha+\frac{1}{2}}}\,\mathbf{dx_2}. \tag{32}$$

For convenience, we use D_p and D_s to denote the nozzle exit diameters of the primary and secondary jet (see figure 4) and u_p and u_s to denote the fully expanded velocities. In (32), $p_a(\mathbf{x_2},\mathbf{x},\omega)$ is the adjoint Green's function and $\omega=2\pi f$ is the angular frequency. For an installed jet, the computation of the adjoint Green's function is not straightforward. Here it is computed using a time domain approach. The adjoint Green's function includes the presence of the wing-flap and thus accounts for sound reflection by these surfaces. $\Gamma(\alpha)$ is the Gamma function. $\bar{u}$ is the mean flow velocity of the jet at the source point $\mathbf{x_2}$. p_{ref} is the reference pressure for the dB scale. a_∞ is the ambient sound speed. The quantities (q_s^2/c^2), α, ℓ_s and T_s are related to k and ε of the k–ε turbulence model as follows,

$$\alpha = \frac{1}{2} + \begin{cases} c_\alpha \dfrac{k^{\frac{3}{2}}}{\varepsilon}\dfrac{1}{\varepsilon}\dfrac{\left|(\nabla u)\cdot(\nabla\varepsilon)\right|}{|\nabla u|} \\ 0 \end{cases} \quad \begin{matrix} \text{(33a)} \\ \text{(33b)} \end{matrix}$$

$$\frac{\hat{q}_s^a}{c^2} = A^2q^2 + \begin{cases} B\dfrac{k^{\frac{3}{2}}}{\varepsilon}\dfrac{1}{\varepsilon}\dfrac{\left|(\nabla u)\cdot(\nabla\varepsilon)\right|}{|\nabla u|}q^2 \\ 0 \end{cases} \quad \begin{matrix} \text{(34a)} \\ \text{(34b)} \end{matrix}$$

$$\ell_s = c_\ell\frac{k^{\frac{3}{2}}}{\varepsilon} + \begin{cases} c_{\ell\alpha}\dfrac{k^3}{\varepsilon^2}\dfrac{1}{\varepsilon}\dfrac{\left|(\nabla u)\cdot(\nabla\varepsilon)\right|}{|\nabla u|} \\ 0 \end{cases} \quad \begin{matrix} \text{(35a)} \\ \text{(35b)} \end{matrix}$$

$$\tau_s = c_\tau\frac{k}{\varepsilon} + \begin{cases} c_{\tau\alpha}\dfrac{k^{\frac{5}{2}}}{\varepsilon^2}\dfrac{1}{\varepsilon}\dfrac{\left|(\nabla u)\cdot(\nabla\varepsilon)\right|}{|\nabla u|} \\ 0 \end{cases} \quad \begin{matrix} \text{(36a)} \\ \text{(36b)} \end{matrix}$$

In (33) to (36), the (a) formulas are to be used when $(\nabla u)\cdot(\nabla r)$ is negative, otherwise the (b) formulas are used. The three constants A, c_ℓ and c_t were determined empirically by Tam & Auriault[11] and they were assigned the values

$$A = 0.755, \qquad c_\ell = 0.256, \qquad c_\tau = 0.233.$$

The remaining four constants were given the values

$$c_{\square} = 2.1599, \qquad B = 0.806, \qquad c_{\ell\square} = \square 0.026, \qquad c_{\square\square} = \square 0.2527$$

in Ref. [12].

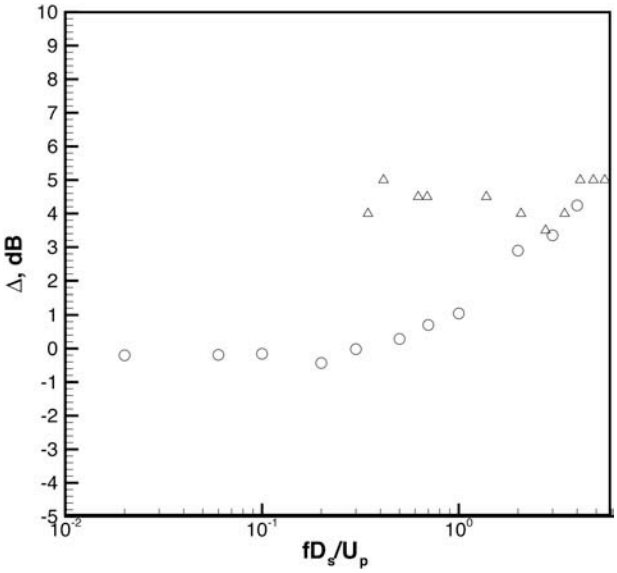

Figure 7. Installation noise. Flap deflection angle 35°. Inlet angle □=90.0°. M_p=0.762, T_p/T_a=2.9; M_s=0.9, T_s/T_a=1.2, M_f=0.28. Area ratio 3, bypass ratio 6 dual stream nozzle. ○ computed. □ experiment.

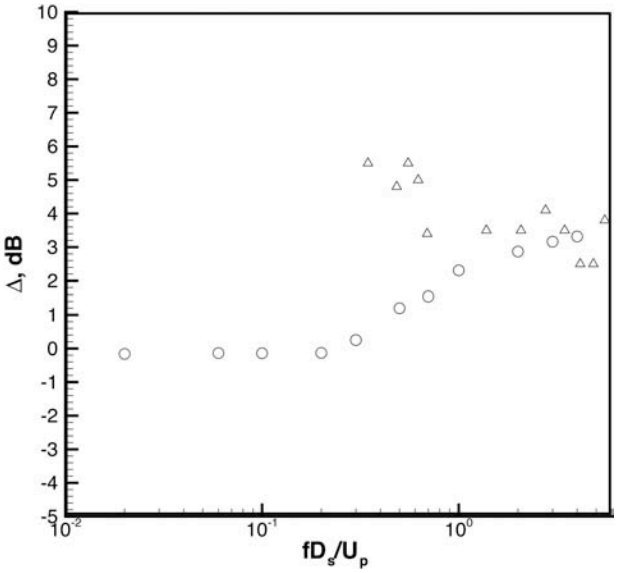

Figure 8. Installation noise. Flap deflection angle 35°. Inlet angle □=120.0°. M_p=0.762, T_p/T_a=2.9; M_s=0.9, T_s/T_a=1.2, M_f=0.28. Area ratio 3, bypass ratio 6 dual stream nozzle. ○ computed. □ experiment.

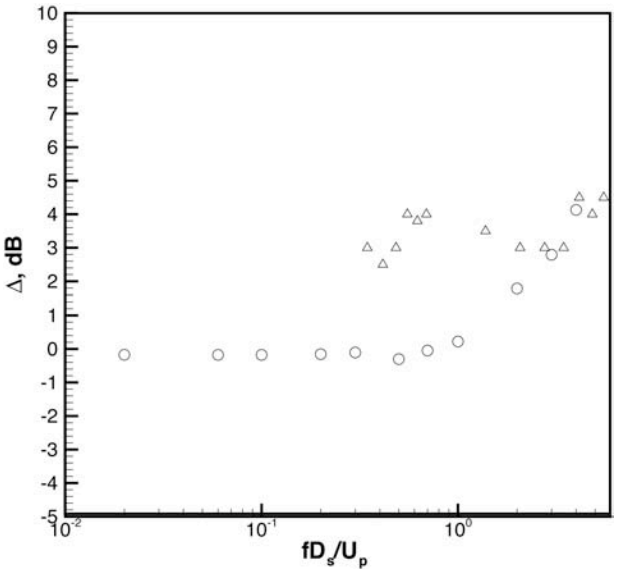

Figure 9. Installation noise. Flap deflection angle 23°. Inlet angle □=90.0°. M_p=0.762, T_p/T_a=2.9; M_s=0.9, T_s/T_a=1.2, M_f=0.28. Area ratio 3, bypass ratio 6 dual stream nozzle. ○ computed. □ experiment.

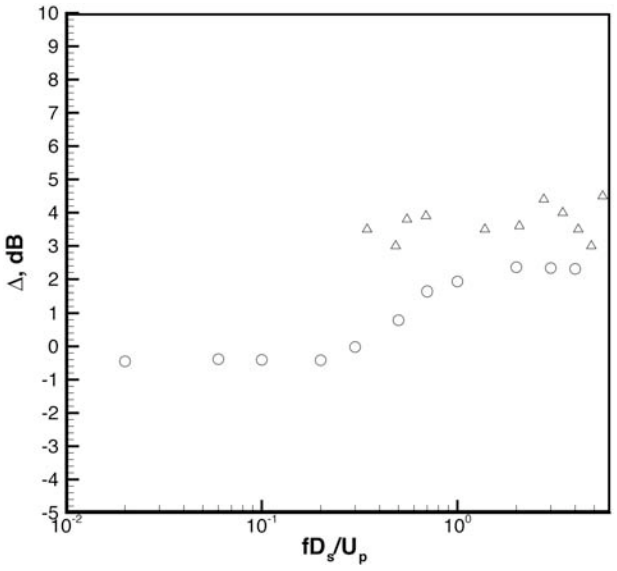

Figure 10. Installation noise. Flap deflection angle 23°. Inlet angle □=120.0°. M_p=0.762, T_p/T_a=2.9; M_s=0.9, T_s/T_a=1.2, M_f=0.28. Area ratio 3, bypass ratio 6 dual stream nozzle. ○ computed. □ experiment.

By means of formulas (30) and (31), the noise of the installed jet whose mean flow velocity profiles are given in figures 5 and 6 are computed. By subtracting out the noise of the same jet in isolation, the installation noise,

□, is found. Figure 7 shows a comparison of the computed installation noise spectrum from the fine scale turbulence of the jet and experimental measurements of Bhat & Blackner[8]. The flap is at a deflection angle of 35°. The measurement microphone is at an inlet angle of 90° in the fly-over plane. As can be seen, the computed installation noise spectrum at high Strouhal number is in good agreement with measurements. However, at intermediate Strouhal number, the measured spectrum has a high level of installation noise that is not predicted by the present model. Figure 8 shows similar comparison at an inlet angle of 120°. There are similar agreement and disagreement with measurements as at 90° inlet angle. Figures 9 and 10 show similar comparisons at a flap deflection angle of 23°. Again similar results as at 35° deflection angle are found.

Clearly, the present model does not predict a mid-Strouhal number increase in installation noise. However, we believe that the mid-Strouhal number installation noise is from the large turbulence structures of the jet flow. For this reason, the present fine scale turbulence noise model is unable to correctly predict the entire installation noise spectrum. It is to be noted that large turbulence structures noise of a jet generally peaks at a lower Strouhal number than that of the fine scale turbulence noise. These large turbulence structures have a near pressure field that extends well outside the jet. This extended field moves downstream with the large turbulence structures. They impinge on the flap when it is deployed at a large angle. The interaction with the flap leads to acoustic scattering and hence noise radiation. We believe this is the mechanism responsible for the observed mid-Strouhal number installation noise. If this explanation is accepted, then the prediction of the present model is in good agreement with experimental measurements. This may also be interpreted as providing a confirmation of the original finding of Ref. [9] that the downwash from the wing-flap has a dominant effect on installation noise.

V. Summary and Conclusions

In this work, the effect of the downwash from a wing-flap combination on an under-the-wing mounted dual stream jet is investigated. It is found that at large flap deflection angle, the jet flow is forced downward and distorted laterally. The deflected jet flow is computed using a set of parabolized RANS equations with a modified *k–e* turbulence model. Numerical results reveal that there is an increase in turbulence level in the jet flow. The noise radiated by the fine scale turbulence of the jet is then calculated by means of the extended Tam & Auriault theory[11,12]. By subtracting out from the computed noise spectrum the noise of the same jet in a stand-alone condition, the installation noise from the fine scale turbulence of the jet is determined.

Comparisons between calculated installation noise and experimental measurements are made. It is found that there are good agreements at the high Strouhal number range. However, measurements indicate significant level of installation noise in the mid-Strouhal number range that is not predicted by the computation. It is, however, the contention of the authors that the discrepancy is not a fault of the computational model, rather that the mid-Strouhal number installation noise is generated by a different mechanism that is beyond the scope of the present investigation. In a jet flow, both large turbulence structures and fine scale turbulence generate noise. The dominant frequencies of large turbulence structures noise are known to be lower than that of the fine scale turbulence. In addition, large turbulence structures of a jet have pressure fields extending well outside the jet. The scattering of the extended pressure field by a deployed flap as the large turbulence structures propagate downstream is believed to be the mechanism responsible for generating the mid-Strouhal number installation noise.

Finally, it is the authors' belief that there is now a computational model by which high frequency installation noise from fine scale turbulence of an installed jet may be computed. Because only a limited amount of experimental data is available at the present time, it has not been possible to perform extensive validation of the computation model. Further comparisons are beneficial and necessary. In addition, there is a great need for the development of a large turbulence structures jet noise prediction theory. In the absence of such a theory, a complete prediction of installation jet noise would be very difficult if not impossible.

Acknowledgment

This work was supported by NASA Langley Research Center Contract NAS1-01045.

References

[1]Way, D.J. & Turner, B.A. 1980 Model tests demonstrating under-wing installation effects on engine exhaust noise. AIAA Paper 80-1048.

[2]Wang, M.E. 1980 Wing effect on jet noise propagation. AIAA Paper 80–1047.

[3]Reddy, N.N. & Tanna, H.K. 1980 Installation effects on jet noise in flight. AIAA Paper 80–1044.

[4]Stevens, R.C.K., Bryce, W.D. & Szewczyk, V.M. 1983 Model and full-scale studies of the exhaust noise from a bypass engine in flight. AIAA Paper 83–0751.

[5]Mead, C.J. & Strange, P.J.R. 1998 Under-wing installation effects on jet noise at sideline. AIAA Paper 98–2208.
[6]Shivashankara, B.N. & Blackner, A.M. 1997 Installed jet noise. AIAA Paper 97–1601.
[7]Blackner, A.M. & Bhat, T.R.S. 1998 Installation effects on coaxial jet noise - an experimental study. AIAA Paper 98–0080.
[8]Bhat, T.R.S. & Blackner, A.M. 1998 Installed jet noise prediction model for coaxial jets. AIAA Paper 98–0079.
[9]Bhat, T.R.S. 1998 Jet-flap installation noise. NASA Contractor Final Report on Contract NAS 1-20267, Task 17, Subtask 2. January 1998.
[10]Lu, H.Y. 1986 An empirical model for prediction of coaxial jet noise in ambient flow. AIAA Paper 86–1912.
[11]Tam, C.K.W. & Auriault, L. 1999 Jet mixing noise from fine scale turbulence. *AIAA J.*, **37**, 145–153.
[12]Tam, C.K.W., Pastouchenko, N.N. & Viswanathan, K. 2004 Fine scale turbulence noise from hot jets. AIAA Paper 2004-0362, January, 2004.
[13]Tam, C.K.W. & Kurbatskii, K.A. 1993 Multi-size-mesh multi-time-step dispersion-relation-preserving scheme for multiple-scales aeroacoustics problems, International Journal of Computational Fluid Dynamics, Vol. 17, No. 2, pp 119-132.
[14]Kurbatskii, K.A. & Tam, C.K.W. 1997 Cartesian boundary treatment of curved walls for high-order computational aeroacoustics schemes. AIAA Journal, Vol 35, No.1, pp. 133-140.
[15]Tam , C.K.W. & Webb, J.C., 1993 Dispersion-relation-preserving finite difference scheme for computational acoustics, Journal of Computational Physics, Vol.,107, Aug. pp. 262-281.
[16]Tam, C.K.W. & Dong, Z. 1996 Radiation and outflow boundary conditions for direct computation of acoustic and flow disturbances in a nonuniform mean flow, Journal of Computational Acoustics, Vol. 4, No. 2, pp. 175-201.
[17]Pope, S.B., 1978 An explanation of the turbulent round jet/plane jet anomly, AIAA Journal, Vol. 16, No. 3, 279-281.
[18]Sarkar, S. & Lakshmanan, B., 1991 Application of a Reynolds stress turbulence model to the compressible shear layer, AIAA Journal, Vol. 29, No. 5, 743-749.
[19]Tam, C.K.W. & A. Ganesan, 2004 A modified k-e turbulence model for calculating the mean flow and noise of hot jets, AIAA Journal, Vol 42, No. 1, 26-34.
[20]Thies, A.T. & Tam, C.K.W., 1996 Computation of turbulent axisymmetric and nonaxisymmetric jet flows using the k-e model, AIAA Journal, Vol. 34, No. 2, 309-316.
[21]Tam, C.K.W., Pastouchenko, N.N. & Auriault, L., 2001, Effects of forward flight on jet mixing noise from fine scale turbulence, AIAA Journal, Vol 39, 1261-1269.
[22]Tam, C.K.W. & Pastouchenko, N.N., Fine scale turbulence noise from dual stream jets, AIAA Paper 2004-2871, May 2004.